Experiments in Fluids 10, 213–223 (1991)

Experiments in Fluids

A cross-correlation technique for velocity field extraction from particulate visualization

T. Utami and **R. F. Blackwelder**

Dept. of Aerospace Engineering, University of Southern California, USA

T. Ueno

Ujigawa Hydraulics Laboratory, Kyoto University, Japan

Abstract. A rapid time series of photographs of the horizontal cross-sections of several y^+ locations were taken of a turbulent open-channel water flow with $Re_d = 3{,}900$. A pair of photographic images were obtained with a time difference of 1.3 ν/u_τ^2 at each y^+ locations. The pictures were digitized into 8 bit data with a spatial resolution of 2.5 viscous scales. Instead of identifying discrete particles, a variable interval spatial correlation technique was used to extract the velocity components. With this technique, two-dimensional spatial cross-correlations of the illumination intensities were taken between a pair of picture images. The correlations were taken over small areas and the peak of the correlation coefficients were used to obtain the convection velocity yielding the u and w components of velocity. Some statistical properties were calculated and are shown to be comparable with previous data. Spatial correlations of the velocity components revealed some unique characteristics related to the structure of turbulence.

1 Introduction

Flow visualization has often been the catalyst for new developments in fluid dynamics; e.g. von Karman's theory of the vortex street, Prandtl's mixing length theory, Reynolds' experiment of transition and more recently various study on coherent structure of turbulence etc. The technique of digitizing pictures and image processing has enhanced flow visualization methods greatly because this technique can now provide quantitative information as well as an encompassing view of the flow structures.

To obtain the two dimensional velocity distribution in a plane by image processing methods, several different techniques have been proposed. One of the most effective methods is to obtain the local correlation of two image patterns having a short time interval between them. By forming the spatial correlation over a small area, the spatial separation giving the maximum correlation identifies the local convection velocity of the particles.

This method was first applied by Kinoshita (1967) before modern day image processing was introduced. He obtained two-dimensional information of velocity vectors on the surface of a flood flow in a river by the manual operation of a stereograph-image plotter. Yano (1983) applied this technique to one bit video image data of 256×256 pixels and obtained the velocity at 64 points. Utami et al. (1990) enhanced this method and applied it to the wall region of a turbulent channel flow. They digitized two photographs into $2{,}000 \times 3{,}000$ pixels each, located individual particles and transformed the particle images into similar patterns. The displacement of these patterns within a small area was used to obtain the velocity ascribed to that area. Thus approximately 3,000 velocity vectors were obtained in an area of 35 cm by 20 cm.

The use of lasers for illumination has led to the development of pulsed laser velocimetry. In its generic form, this technique uses a doubly exposed photographic film of particles in a flow field with an illumination source density less than unity. Adrian and Yao (1984) introduced an auto-correlation analysis to extract the velocity field. Small areas of the photographs were autocorrelated in a manner originally suggested by Kovasznay and Arman (1957). The maximum of the correlation is used to identify the local convection velocity assigned to the area. The method and other aspects of particle image velocimetry have been analyzed by Adrian (1988).

In this paper, the second series of the set of photographs described by Utami et al. (1990) was analyzed using the pulsed image velocimetry but with the following differences. First, two different photographic images are utilized necessitating the use of cross-correlation instead of auto-correlations. Secondly a more moderate particle density allowed the entire photographs to be digitized and stored. This allowed greater flexibility in algorithm development and the image intensity field could be displayed and compared with the original data. This was especially useful for finding an optimum averaging area for the correlations.

The technique assumes that each pixel has several bits of resolution so that the digitized image provides a continuous field of illumination. Standard correlation methods are used to correlate small spatial areas of the illumination field with like regions in another image taken at a slight time difference. The spatial resolution of the method is determined by the size of the correlated area and can be made small. On the

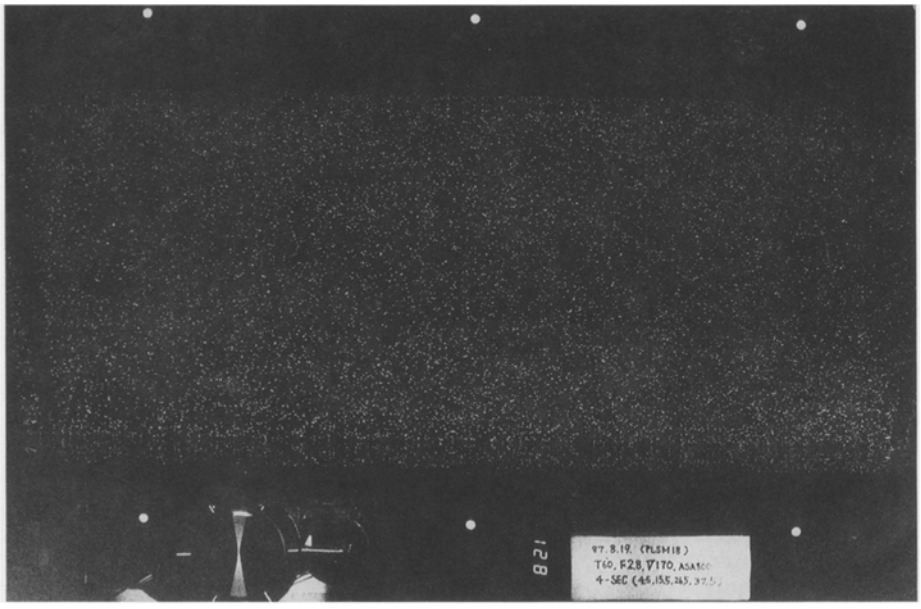

Fig. 1. Photograph of particles in the channel flow; the sides of the channel are inside the six bright reference dots

other hand, the correlated area must be sufficiently large so that the image of more than one particle is included in it; otherwise an ambiguity will result. The method offers an experimental technique capable of obtaining the entire velocity field of complicated three-dimensional flow fields as discussed by Utami et al. (1990).

2 Experimental method

A rapid time series of photographs of the horizontal cross-sections at several y^+ locations were taken of a turbulent open-channel water flow. The visualization method used polystyrene beads with an average diameter of 0.4 mm and a 3 mm thick sheet of white light. A pair of photographic images were obtained with a time difference of $1.3\ \nu/u_\tau^2$ at each y^+ locations. Eighteen pairs of photographs were taken from the channel bed to the water surface and the procedure was repeated four times in rapid succession to yield four series of photographs.

The details of the experimental method and some results obtained from processing the first five pairs of photographs in the first series were described by Utami et al. (1990) by using particle tracking methods. In the present paper, particle image velocimetry method was used to analyze the five pairs of the photographs in the second series.

An example of original photographs that were digitized for this analysis is shown in Fig. 1. The photographs were always taken in pairs and the actual time between photographs was obtained from the clock seen at the lower left hand corner in Fig. 1. The physical coordinates of the images were calculated using the six reference marks in the photographs which appear as the six large bright dots in the figure external to the channel. The friction velocity u_τ, obtained from separate measurements of the slope of energy head was 0.57 cm/s. The water channel had a width of 40 cm, and the water depth was 3.95 cm. The photographs were taken 7.5 m downstream of the entrance to the uniform test section. The Reynolds number based upon the water depth and average velocity was 3,900. The coordinate system was chosen so that the x axis was aligned with the mean flow direction, y was perpendicular to the wall and z was in the spanwise direction. The respective velocities are denoted by u, v and w.

Table 1. Flow conditions in each plane

y^+	8	21	37	53	68
y (cm)	0.115	0.31	0.54	0.77	1.00
U_m/u_τ	9.8	14.2	14.8	14.9	15.7
u'/u_τ	2.70	1.93	1.92	1.47	1.64
w'/u_τ	0.98	0.99	1.06	0.95	1.08
S_u	0.27	−0.09	−0.12	−0.09	0.01
S_w	−0.21	−0.06	0.00	−0.01	−0.08
F_u	2.72	2.35	2.60	2.62	2.86
F_w	3.72	3.10	3.23	3.31	3.21
a	5.00	4.00	2.00	1.50	1.50

The analysis was limited to a 40 cm × 24 cm area which was the central part of the channel in the right half of the photographs. The origin of the coordinates was taken near the midpoint of the picture in the streamwise direction and 10 cm from the channel wall. The resulting flow parameters of each analyzed plane are listed in Table 1. U_m is the mean velocity in the plane, u' and w' are the turbulence intensities, S_u and S_w are the skewness factors for u and w, and F_u and F_w are the corresponding flatness factors. All the u and w velocity data were obtained from the two-dimensional vector data before interpolation. The parameter a is described in the interpolation section.

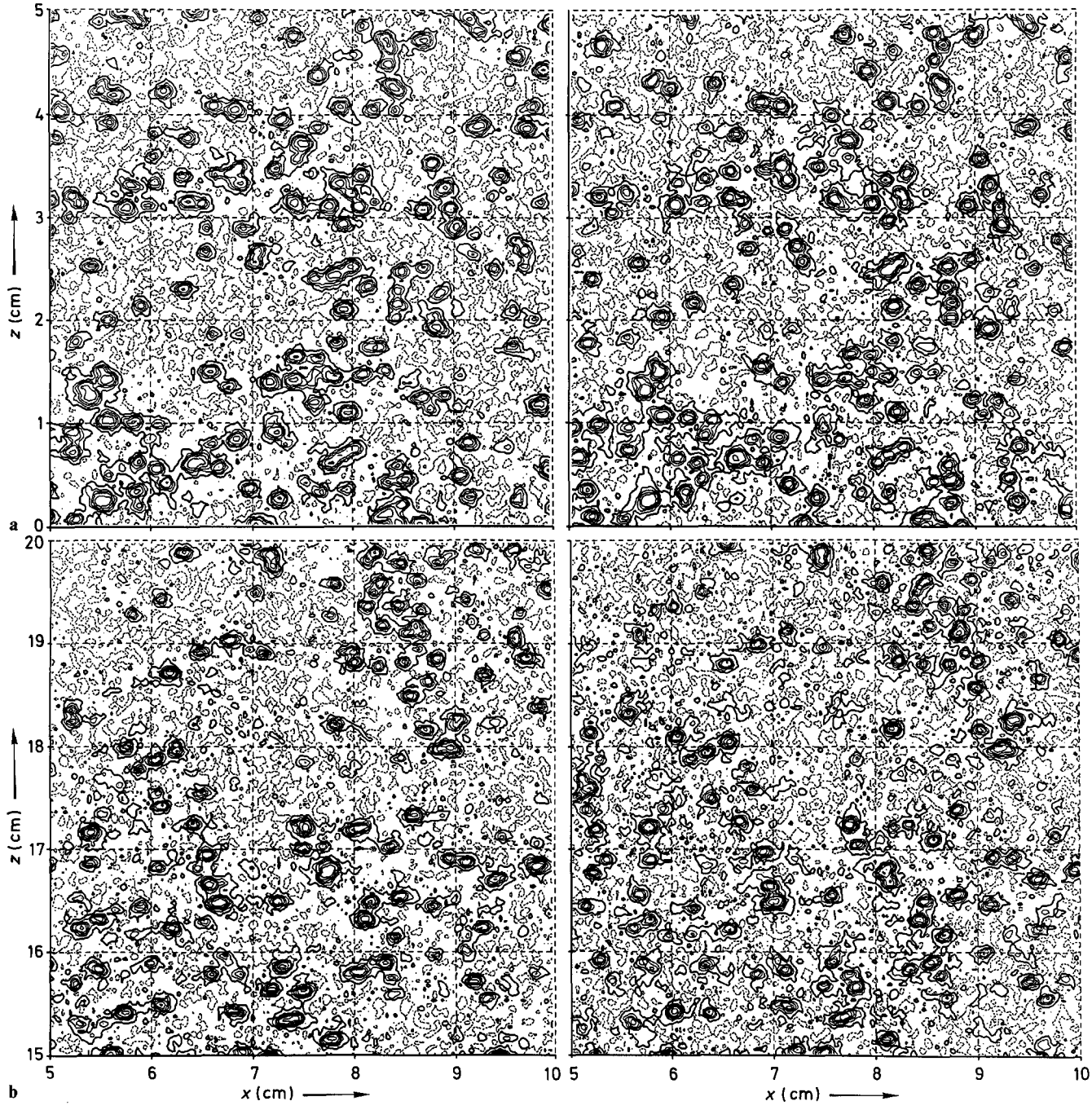

Fig. 2. **a** The illumination intensity from a region with relatively high particle concentrations; the figure on the right was taken at time Δt after the one on the left; **b** the illumination intensity from a region with relatively low particle concentrations; the figure on the right was taken at time Δt after the one on the left

3 Image Processing

3.1 Digitization

The photographs were digitized into 8-bit digital data by an Optronics C-4100 HS drum scanner in the Signal and Image Processing Institute of the University of Southern California. The digitizing resolution was 0.1 mm from the photographs which corresponded to an actual physical size of 0.37 mm ($2.5\ v/u_\tau$). Figure 2a are plots of the illumination intensity from a pair of photographs separated by a time Δt taken from an area with a high density of tracer particles. Figure 2b is taken from the same photographs but in an area with a lower density of particles. The heavier lines indicate the mean value of the light intensity of the corresponding areas. The lighter solid lines are the regions where the light intensity exceeded the mean value and identify the location of the particles. The interval between the contour lines repre-

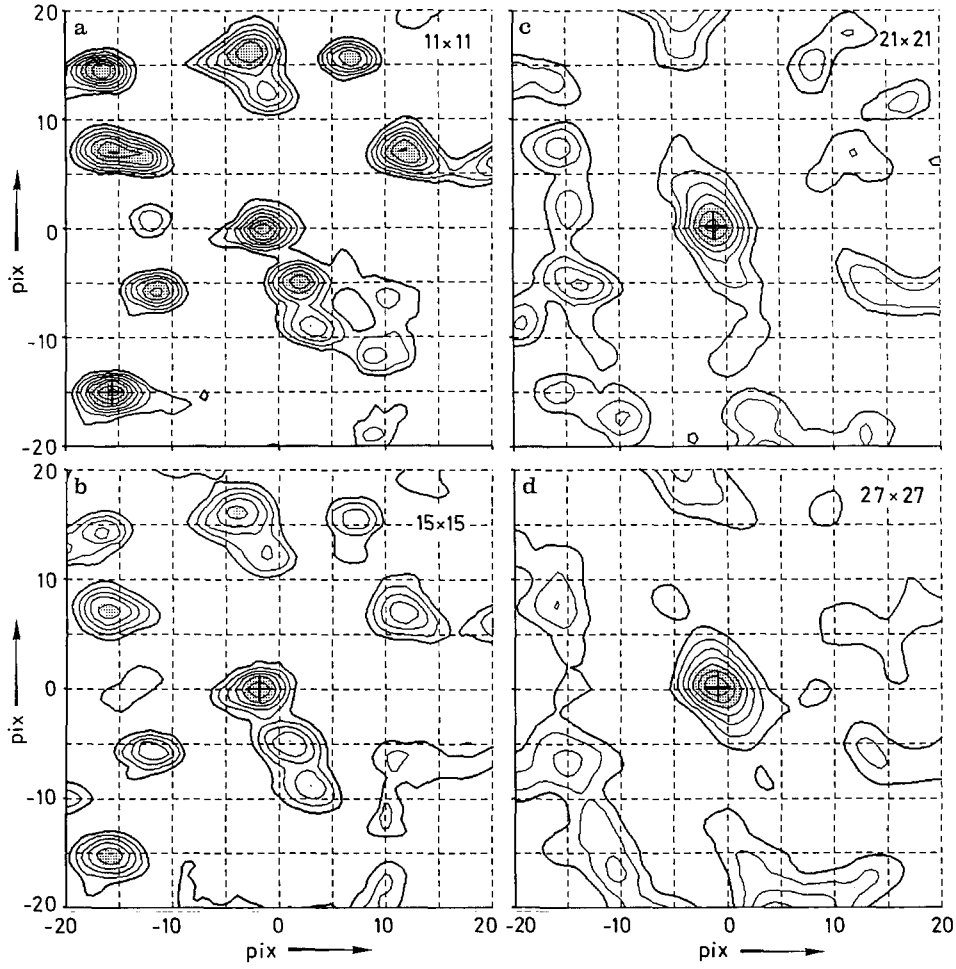

Fig. 3a–d. Isocorrelation contours for four different pattern areas of sizes **a** 11×11, **b** 15×15, **c** 21×21 and **d** 27×27 pixels; The shaded areas have correlation coefficients greater than 0.5

sents one rms of the light intensity over the area. The dashed lines indicate those regions where the intensity was below the mean value. Careful examination of the figure indicate that the high intensity regions are much more strongly peaked than the areas of low intensity; i.e. the intensity signal is strongly skewed positively. Examination of the pairs shows that each of the particles have moved a distance corresponding roughly to the mean velocity.

3.2 Reference coordinates

Six reference marks on the exterior of the channel were illuminated separately and recorded in the photographs. Their coordinates were measured precisely beforehand and used to obtain the physical coordinates of each pixel. The digital image of the reference marks was not always an exact circle but had slight imperfections due to the non-uniformity of the grain structure in the photographs. Thus the centers of their images were obtained by a two-dimensional fit to a Gaussian function.

A two-dimensional Gaussian distribution over 21×21 pixels with the standard deviation nearly equal to the radius of the image of the reference marks was correlated with the digitized intensity distribution with the eight bit pixel pattern of the reference marks. The approximate center of the reference marks were determined as the maximum point of the correlation coefficients. A more exact center of the reference marks was obtained by applying an interpolation scheme. The correlation coefficients near the maximum were fit with a two-dimensional second order least squares. The resulting curve was examined to find its maximum which effectively interpolated between the pixel locations. The resulting center for the reference mark was found to within one tenth of a pixel spacing with an error of 0.05 pixel spacings.

3.3 Variable interval spatial correlation analysis

Instead of identifying discrete particles and tracking them from one photograph to the next, two-dimensional correlations of small areas were used to determine the velocity components at each location. First, a small pattern area, typically 21×21 pixels, centered about x_i and z_j was chosen in the first photograph. The two-dimensional cross-correlation of the intensity pattern was then obtained; i.e.

$$R_{II}(x_i, z_j; \Delta x, \Delta z, \Delta t) = \overline{I(x_i, z_j, t)\, I(x_i + \Delta x, z_j + \Delta z, \Delta t)}$$

was computed where $I(x, z, t)$ and $I(x, z, \Delta t)$ are the illumination intensity patterns from the two photographs. x_i and z_j denote the location of the (i, j) pixel. The image in the second photograph was taken at a time Δt later than the first. The correlation was obtained for a range of spatial separations, Δx and Δz, that would include the largest possible excursion due to the velocity components. Since the time between photographs was small, $\Delta t = 1.3\ \nu/u_\tau^2$, the intensity pattern did not change appreciably as seen in Fig. 2 and the maximum correlation coefficients were typically 0.7 and greater.

The location of the maximum correlation value, Δx_{max} and Δz_{max}, were used to determine the velocity of the pattern. Since the correlations could be computed only at integer values of the pixel distance, the location of the correlation maximum, Δx_{max} and Δz_{max}, were found using second-order two-dimensional least squares fit near the peak in the correlation. This method allowed interpolation between the pixel values and improved the velocity resolution. The velocity components at the point (x_i, z_j) were then taken to be $u = \Delta x_{max}/\Delta t$ and $w = \Delta z_{max}/\Delta t$. The velocity computed in this manner is actually the convection velocity of the intensity pattern of the particles, but the time step is so small that it can be taken as the field velocity at the center of the pattern.

The initial size of the correlated area (i.e. the limits placed upon Δx and Δz) is a variable that must be determined. The best size for this pattern area is dictated by the size and concentration density of the particles. The results for four different sizes of the initial pattern are seen in Fig. 3 where the contour levels of the computed cross-correlation are plotted. Each particle generated an image that was typically 5–7 pixels wide. Hence when the pattern area was of the same order as the image of individual particles, any single particle was well correlated with all other particles. In this case, the peaks in the correlation corresponded to not only the correlation between the two images of the same particle, but also to the correlation between the original particle at time $t = 0$ and any other particle in the image at Δt later. Because the particles reflected different amounts of light in the two images, the maximum correlation would often be the result of the correlation between two different particles thus yielding an incorrect velocity. This is seen in Fig. 3a where an initial pattern size of 11×11 was used. Several local peaks are seen in the correlation and the maximum in the lower left hand corner yields an absurd velocity. The reason is that in this case, the 11×11 pattern correlates only discrete particles and not groups of particles.

For pattern areas of 15×15 pixels and greater, the maximum correlation is seen to be at almost the same values of Δx and Δz. For larger areas such that several particles are included in the pattern, the numerous points of high correlation disappear as seen in Fig. 3b–d. For the present conditions, a pattern area of 21×21 pixels was used because there was typically only one strong local peak in the correlation function. Although larger areas could have been used also, they provide a larger averaging area and thus reduce the spatial resolution of the technique. The dependence of the results upon the average number of particles per averaging area has been quantified by Adrian (1988) into a nondimensional parameter N_I. For the 21×21 area, $N_I = 4.0$.

After computing the velocity at the point x_i and z_j, i and j were incremented and the velocity components at the new point were computed. In this investigation, i and j were incremented in steps of 5 to reduce the time required for the calculations. It is noted in Fig. 3 that the maximum correlation is located to the left of the origin indicating a negative mean velocity. This is due to the fact that the second photograph was shifted in the x direction by an amount $U_m \cdot \Delta t$ where U_m is the estimated mean velocity. This placed the most probable location of the correlation peak at the origin and improved the computational efficiency.

3.4 *Refraction correction*

The coordinates of the tracer images are shifted from the physical coordinates by refraction at the water surface. In the present case, the camera was 2.19 m above the channel bed and the refractive shift amounted to 4 mm in the extreme case. Thus the coordinates of both end points of the vectors were corrected so that the effect of the refraction at the water surface was removed by using the law of geometrical optics.

3.5 *Spatial resolution*

With any new method, the spatial resolution is an important parameter. The resolution in Δx and Δz is dictated by the pixel size and the techniqe. The distance between pixels was $2.5\ \nu/u_\tau$ as determined by the digitizing interval. However Browand and Plocher (1985) have shown that the interpolation of the peak of the correlations between pixels provided a resolution of approximately $0.1\ \nu/u_\tau$. The light sheet was $20\ \nu/u_\tau^2$ thick which provides a large Δy resolution. This is unacceptable for obtaining good data near the wall and could be improved upon considerably by using a laser light sheet. The details of the new method should be independent of this resolution. To expedite the development of the new technique, an existing set of data were utilized with the large Δy resolution.

3.6 *Other corrections*

In some regions of the photographs, there was a lower concentration of particles than in others. The intensity pattern in these areas was quite noisy and it produced relatively low correlation values, i.e. typically of the order of 0.3. In these regions, the maximum correlation was often due to random light intensity and was not indicative of the convection velocity at that point. Thus an incorrect velocity was obtained

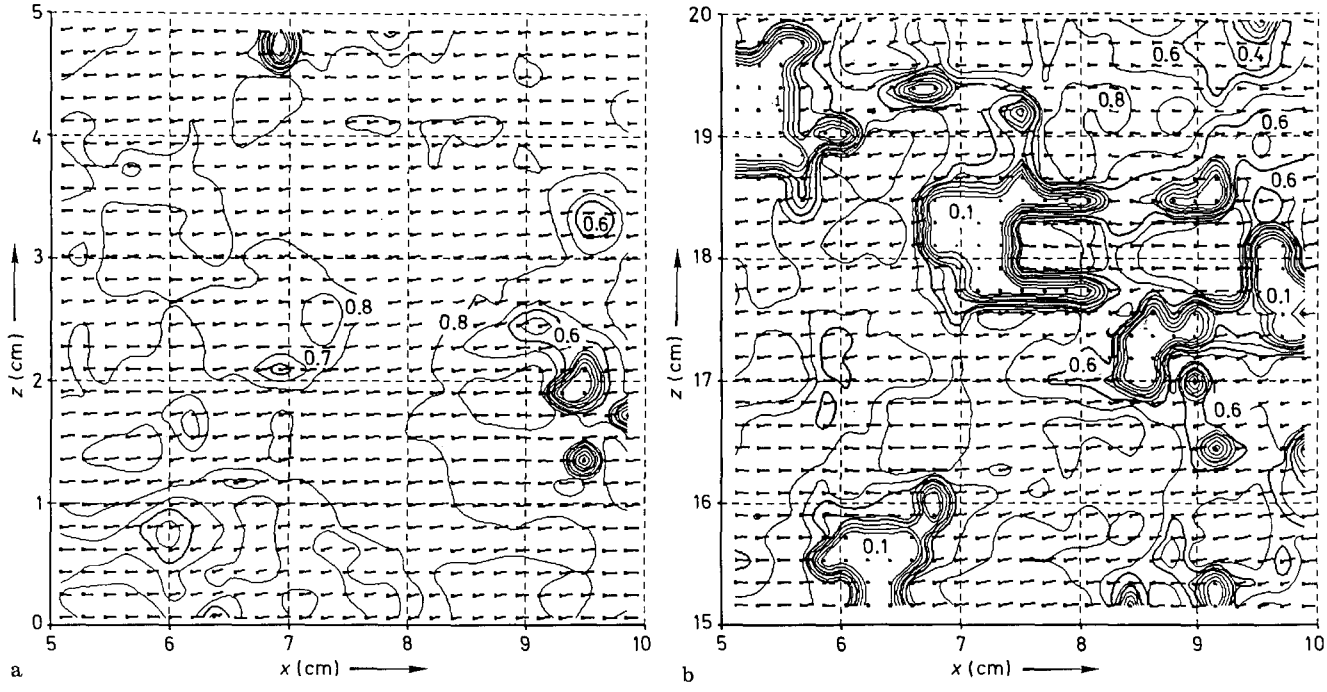

Fig. 4 a and b. Iso-contours of the maximum correlations; **a** on the left and **b** on the right correspond to the data in Figs. 2 a and b respectively; the interval between the contours is 0.1; note that the valid vectors correspond to regions with correlations greater than 0.5

by the above analysis. These questionable vectors were removed by comparison with the local mean velocity. The local mean was calculated at a point by averaging the velocity vectors over a 50×50 pixel area using only those data that had correlation coefficients greater than 0.7. If the streamwise velocity computed at the point differed from its local mean value by more than 30%, it was excluded from all further analysis. Likewise if the ratio of the two velocity components, w/u, exceeded 0.25, the velocities at that point were excluded.

Figure 4 shows the contours of the computed maximum cross-correlation coefficients for the same areas shown in Fig. 2. The interval between the contour lines is 0.1. The resulting velocity vectors from the above analysis are shown by line segments emanating from each (x_i, z_j) location. The questionable vectors that were removed are represented by null vectors. Note that in the regions having null velocity vectors, the correlation is low; i.e. typically less than 0.7 and almost always less than 0.5. Comparing Fig. 4 a with Fig. 2 a, it is seen that valid velocity vectors were obtained almost everywhere. However in Fig. 4 b many velocity vectors are null vectors. Comparing this result with Fig. 2 b it is readily apparent that the regions of null vectors correspond to regions of low particle densities. In addition, Fig. 4 indicates that the regions of the null vectors do indeed correspond to the areas of low correlation.

The rms fluctuation value of the light intensity field can also be computed in several different ways. First this quantity can be calculated over the entire field which yields the usual rms value. However a local value can also be computed to indicate how much the signal in the neighborhood of a point is fluctuating. Figure 5 shows the contours of the rms values computed over a 21×21 pixel area corresponding to Fig. 2 respectively. Each contour level is 2% of the maximum illumination intensity and the heavy lines represent 8% and 16% of the maximum intensity. All of the areas having fluctuations less than 8% are shaded. It is easily seen by comparison with Fig. 2 that regions devoid of particles have the smallest intensity fluctuations. By comparing Figs. 2, 4 and 5, it is clear that the more tracers present in a local region, the larger the rms value of the light intensity and the greater the correlation coefficient. In regions of low rms values, a larger pattern area could have reduced the number of null vectors. However a constant pattern area of 21×21 pixels was used for simplicity.

The velocity vectors computed in the above manner at $y^+ = 21$ are shown in Fig. 6. In order to include the entire field in the figure, only every fifth vector along the x coordinate is plotted. The questionable velocity vectors are represented by the null vectors. More detailed information can be gleaned from Fig. 4 which can be compared with Fig. 6 since their coordinates are the same. By comparing Fig. 6 with Fig. 4 it is apparent from the previous discussion that the regions with null vectors are the regions with a low concentration of particles. The location of the null vectors could also have been determined by examination of the maximum correlation coefficients over the field. From the previous results in Fig. 4 it is apparent that the questionable velocities almost always corresponded with regions having a maximum correlation less than 0.5. To compare this observation with the resulting vectors in Fig. 6, the contours of the maximum correlation coefficients were plotted (not shown). De-

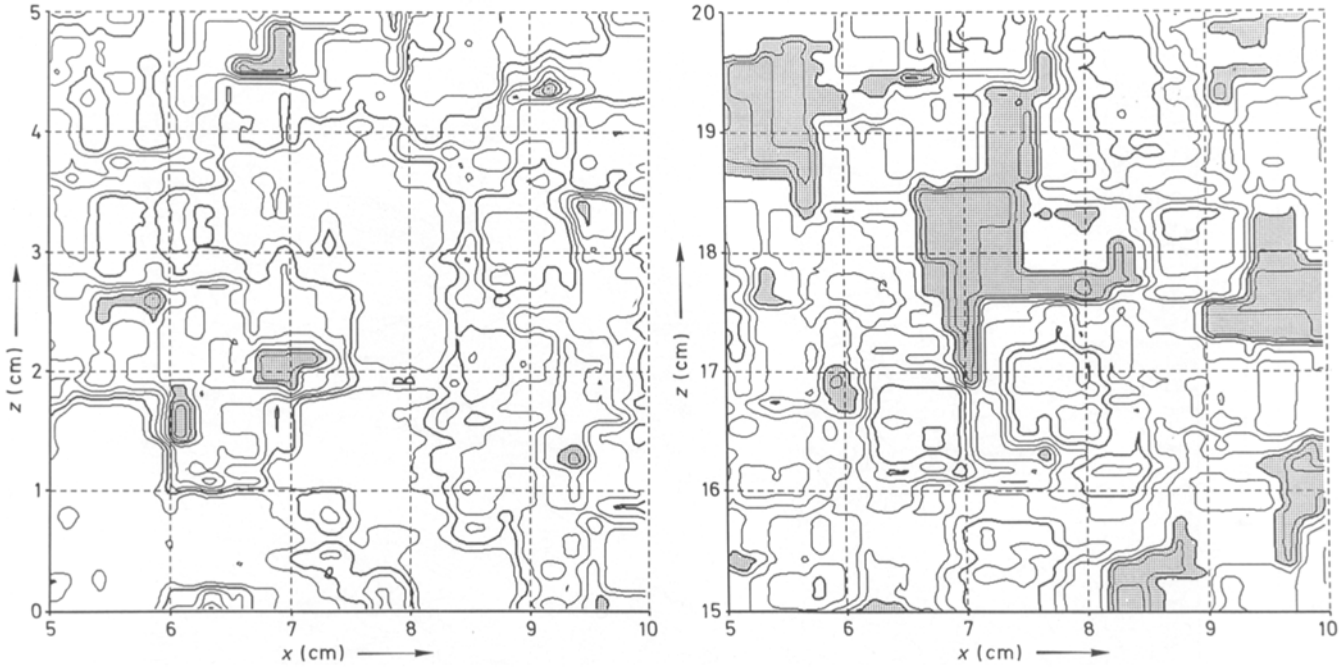

Fig. 5. Contours of the rms light intensity fluctuations corresponding to Fig. 2

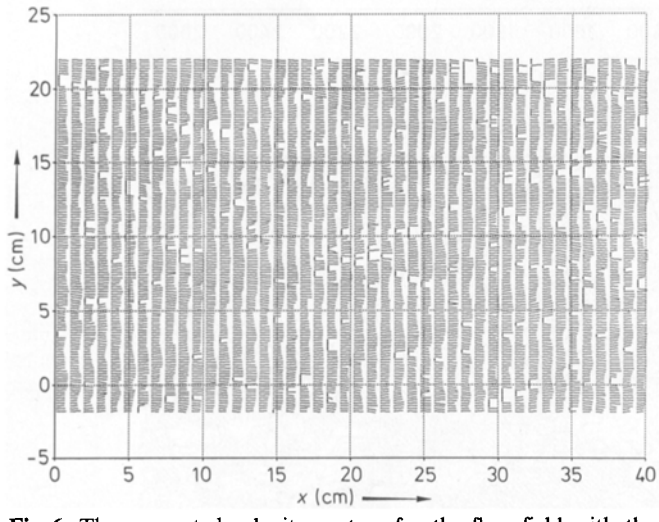

Fig. 6. The computed velocity vectors for the flow field with the questionable velocities represented by null vectors

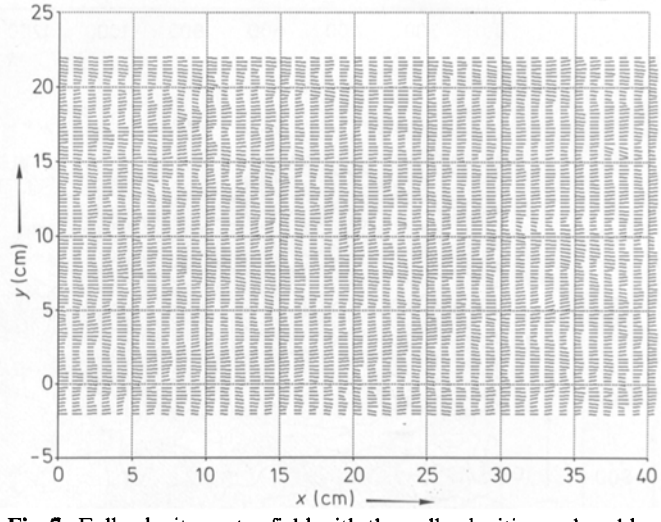

Fig. 7. Full velocity vector field with the null velocities replaced by the interpolated velocity vectors

pending upon the y^+ location, these results found that the maximum correlation coefficients were larger than 0.6 over approximately 90% of the plane. In addition, the null vectors did indeed correspond with those regions having correlation coefficients less than 0.4.

3.7 Interpolation

For convenience in the following analyses, the calculated values of u and w were transformed onto a regular grid with grid intervals of 2.5 mm (17 viscous length scales). The method used is described by Utami et al. (1990). It utilized an elliptical interpolation scheme following the characteristics of R_{uu} and R_{ww} correlations in the wall region which have aspect ratios, a, given in Table 1. The velocity vectors in the $y^+ = 21$ cross-section obtained by the interpolation scheme are shown in Fig. 7. The null vectors have now been replaced by the weighted average value of the vectors obtained from an elliptical area. Since only every fifth vector along the x axis is plotted, Figs. 5 and 7 provide non-repetitious but complimentary information since different values of the index i are plotted.

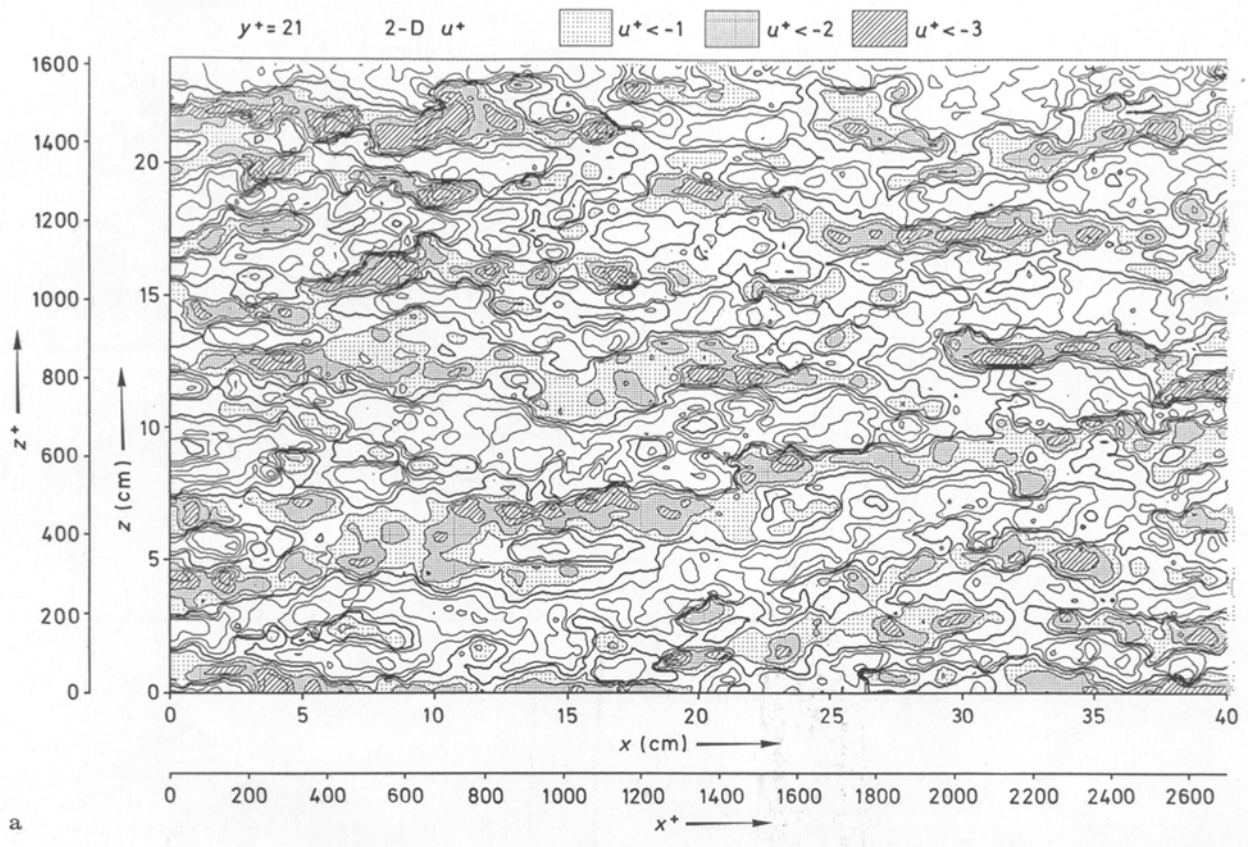

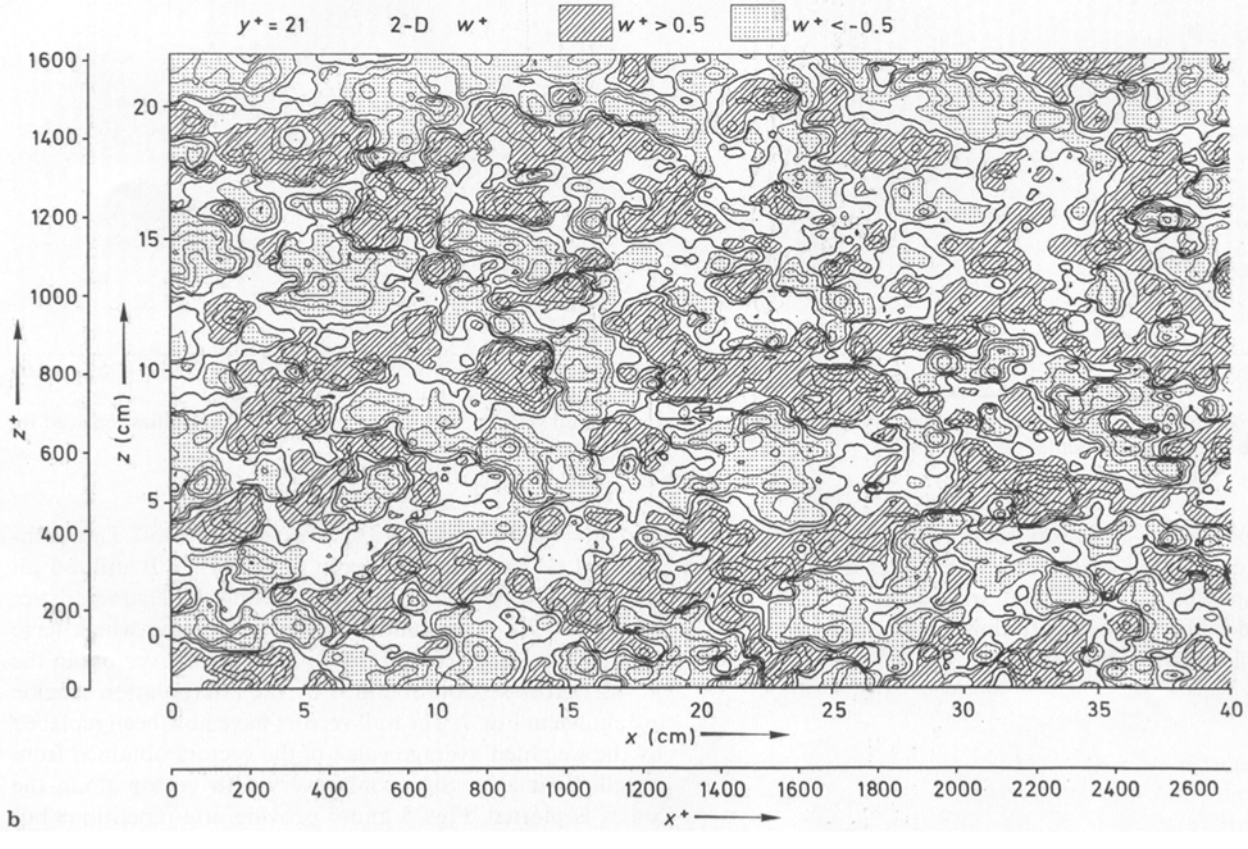

Fig. 8. **a** Iso-velocity contours of the streamwise velocity, u; the shading keys are found at the top of the figure; **b** iso-velocity contours of the spanwise velocity, w; the shading keys are found at the top of the figure

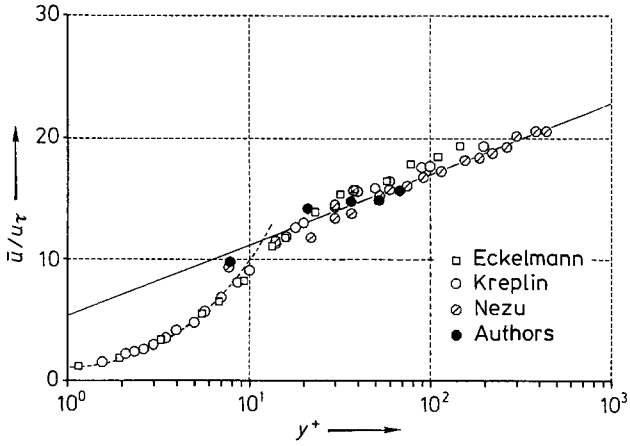

Fig. 9. The mean velocity data compared with the standard log law profile

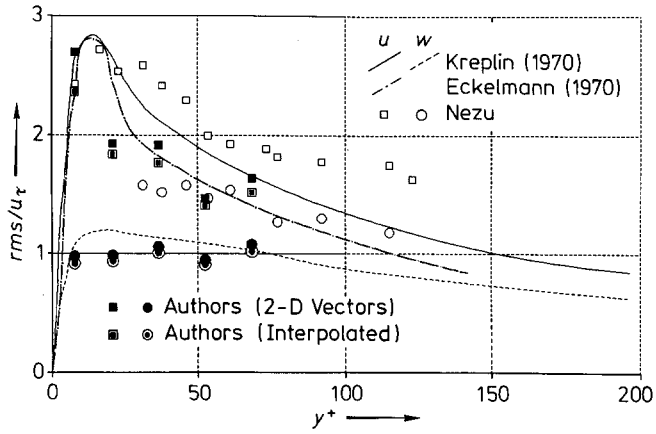

Fig. 10. The rms intensity fluctuations of u and w compared with previous authors data

With a continuous velocity field obtained from the interpolation scheme, the iso-contours of the u and w components of the velocity vectors can be computed and are shown in Fig. 8. To identify the low speed streaks, the low speed part of u component are shaded in Fig. 8a. It is noticeable that the u component has elongated structures while the w component does not have such a characteristic as has been reported by previous authors. However the aspect ratio is not as large as has been reported by Moin and Kim (1982). This is due to the fact that the data in Fig. 8 was taken at $y^+ = 21$, i.e. in a region where the streaks are not as predominant as they are closer to the wall. The small aspect ratio of the streaks in Fig. 8a is probably also due to the relative large area over which the present data were averaged. In that regard the present results are similar to the earlier numerical work at NASA Ames in which the grid spacing were rather coarse, e.g. Kim and Moin (1980). The w velocity component in Fig. 8b has no elongated structure in agreement with the previous results of Moin and Kim (1982) and others.

4 Statistical characteristics

4.1 Average velocity

The average velocity in each plane calculated from the present data was compared with the oil channel data of Eckelmann (1974) and Kreplin (1976) and the open-channel data of Nezu (1977) in Fig. 9. The present data agrees well with the previous authors and follows the logarithmic law with $\varkappa = 0.4$ and $C = 5.5$ shown in the figure.

4.2 Intensity of turbulence

The rms values of turbulence were calculated by two methods; namely the rms of the velocity components was obtained before interpolation and also afterward. These values are presented in Fig. 10 and are compared with Eckelmann's (1970), Kreplin's (1976) and Nezu's (1977) data. The present data agree slightly better with Eckelmann's (1970) and Kreplin's (1976) data. Note that the interpolated data will always yield a smaller value of the rms value as seen. The difference between the two methods of calculating the rms is smaller than the results obtained by using the particle tracking method; see Utami et al. (1990). In their case the raw velocity vectors were computed by individually tracking particles from one photograph to the next. The main reason for the improved results here is that for the present data, approximately 27,000 vector data were interpolated into roughly 15,600 grid point data and hence the smoothing effect was less. This is an important advantage of the present method.

4.3 Two-dimensional spatial correlations

Spatial correlation coefficients of u and w with two-dimensional spatial separations, $R_{uu}(\Delta x, \Delta z)$, and $R_{ww}(\Delta x, \Delta z)$, were calculated from the interpolated data. The correlations at $y^+ = 21$ and 68 are shown in Fig. 11. The heavy solid line denotes the zero correlation locus, the lighter solid lines are positive and the dashed lines are negative correlation. The interval between the isocorrelation contours is 0.1. The contours of the R_{uu} correlation are highly elliptic as Grant (1958), Compte-Bellot (1963) and Moin and Kim (1982) have pointed out. The aspect ratio of the 0.5 correlation contour is 3.9 at $y^+ = 21$ and 2.8 at $y^+ = 68$. On the other hand, the contours of the R_{ww} correlation coefficient are circular, particularly in the cross-section far from the wall. The aspect ratio of the 0.5 contour line is 1.5 at $y^+ = 21$ and 1.1 at $y^+ = 68$.

A more interesting correlation is the cross-correlation, $R_{uw}(\Delta x, \Delta z)$, found in Fig. 12. The interval between the isocorrelation contours is 0.05. In general, most all spatial correlations have some degree of symmetry about the two axes.

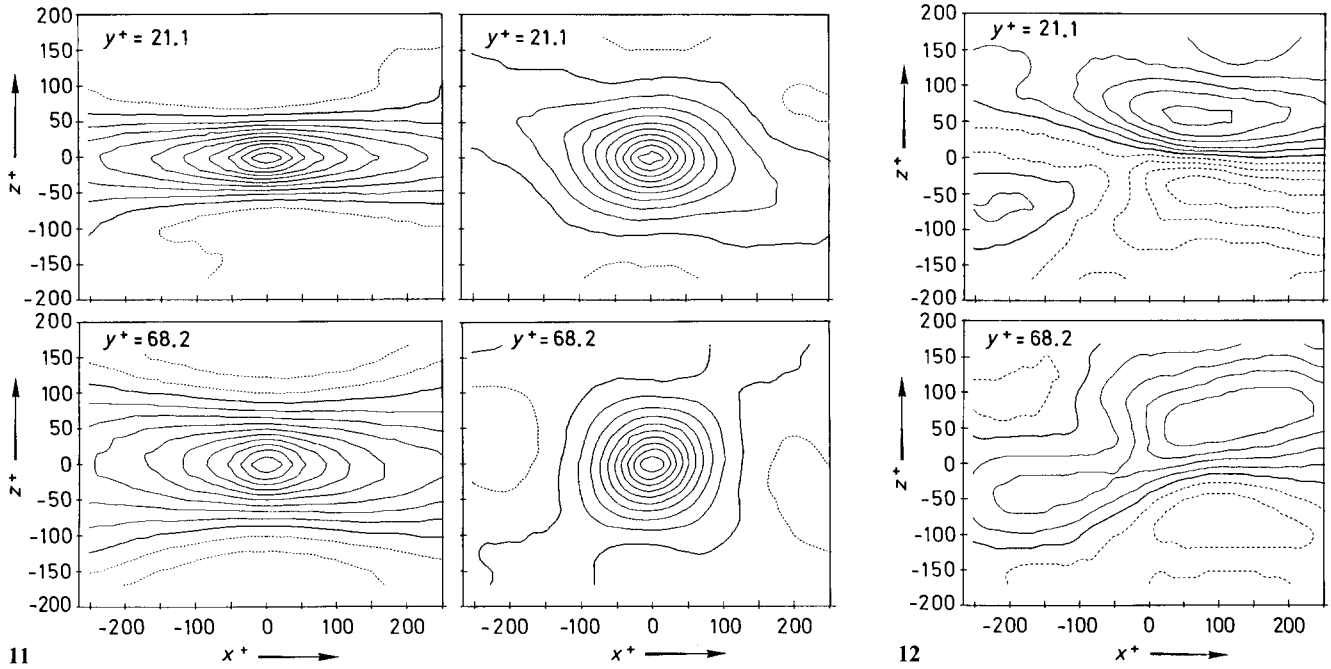

Fig. 11. The R_{uu} (on the left) and R_{ww} (on the right) spatial correlations at $y^+ = 21$ (above) and 68 (below)

Fig. 12. The cross-correlation R_{uw} at $y^+ = 21$ (above) and 68 (below)

In Fig. 12, one can see that the correlation is anti-symmetrical about the x axis. However the R_{uw} correlation does not display any symmetry in the streamwise direction which indicates a unique relationship between these two velocity components. At $y^+ = 21$, the correlation suggests that whenever the u velocity component of the fluid at $\Delta x = 0$ is positive, the fluid downstream, i.e. $0 < \Delta x^+ < 250$, is spreading outward in the spanwise direction. Likewise whenever u component is negative at a point, $\Delta x = 0$, the fluid downstream has spanwise velocities pointing toward the centerline. At the higher elevation, the R_{uw} correlation has become more antisymmetric about both axis and has two distinct positive and negative regions. This shape is similar to the cloverleaf shape of the correlation between the intermittency function and the spanwise velocity found by Blackwelder and Kovasznay (1972) in the outer portion of a turbulent boundary layer. This type of a correlation pattern could be due to the low speed fluid rising from the wall region. As it passes through the $y^+ = 68$ level, the relatively higher speed fluid surrounding it must pass around it as well as mixing with it. As the surrounding fluid passes, the spanwise velocity must be diverging upstream and converging downstream yielding the pattern seen in Fig. 12.

5 Conclusions

The results show that the new variable interval spatial correlation technique can be used to obtain the velocity field from small tracers used in flow visualization. Although only the u and w velocity components were obtained in the present results, there is no reason that the method can not be extended to include the v component as shown by Utami et al. (1990).

The present results were produced from visualization data originally obtained for particle tracking and were thus not optimized for the new technique. The method could be improved by the optimization of several experimental parameters. The size of the particles could be reduced slightly and their concentration increased. Also a narrower sheet of light such as a laser sheet could be used. Both of these suggestions would improve the spatial resolution of the method. The mere fact that the present results could be obtained illustrates on of the advantages of the method; i.e. that it can be adapted to a large variety of experimental parameters by changing the variables such as the pattern size and the area interval over which the correlations are calculated.

The method is also rather flexible in terms of calculating the validity of the deduced velocity vectors. For example, only the magnitude of the calculated correlations were used in the present results to ascertain the accuracy of the vectors. However Figs. 2, 4 and 5 indicate that different algorithms could be developed and used that would utilize other parameters such as the relative density of the particles, the rms of the illumination intensity, etc. in order to determine regions where high uncertainty exists in the calculated velocity vectors.

The method was used to calculate the two-dimensional spatial correlations found in Figs. 11 and 12. The cross-cor-

relation, R_{uw}, had a very characteristic shape associated with the eddy structure near the wall. It indicated that when u was less than its mean (such as in a low speed streak), the spanwise velocity downstream was converging towards the line of symmetry. Likewise when the streamwise velocity was greater than its mean, the downstream pattern for the spanwise velocity was one of divergence.

Acknowledgements

The authors thank L. Durham and A. Weber for assisting in digitizing the original photographs. The support of the AFOSR is gratefully acknowledged under contract no. F49620-85-C-0080 monitored by J. McMichael for that portion of the research conducted at USC.

References

Adrian, R. J. 1988: Statistical properties of particle image velocimetry measurements in turbulent flow. In: Laser anemometry in fluid mechanics. (Eds. R. J. Adrian, T. S. Asanuma, D. F. G. Durao, F. Durst and J. H. Whitelaw). pp 115–129

Adrian, R. J.; Yao, C.-S. 1984: Development of pulsed laser velocimetry for measurement of turbulent flow. In: Symp. of Turbulence. (Eds. Reed, X. B.; Patterson, G. K.; Zakin, J. L.). pp. 170–186. Symposium held at University of Missouri, Rolla, Missouri, Published by Chem. Eng. Department

Blackwelder, R. F.; Kovasznay, L. S. G. 1972: Time scales and correlations in a turbulent boundary layer. Phys. Fluids 9, 1545–1554

Browand, F. K.; Plocher, D. A. 1985: Image processing for sediment transport. In: Proc. 21st Congr. Int. Assoc. for Hydraulic Research, pp 8–14, Vol. 5, Congress held at Melbourne, Australia

Compte-Bellot, G. 1963: Contribution a l'etude de la turbulence de conduit. Ph.D. Thesis, University of Grenoble

Eckelmann, H. 1970: Experimentelle Untersuchungen in einer turbulenten Kanalströmung mit starken viskosen Wandschichten. Mitteilungen Nr. 48, Max-Planck-Institut für Strömungsforschung und der Aerodynamischen Versuchsanstalt, Göttingen, F. R. Germany

Eckelmann, H. 1974: The structure of the viscous sublayer and the adjacent wall region in a turbulent channel flow. J. Fluid Mech. 65, 439–459

Grant, H. L. 1958: The large eddies of turbulent motion. J. Fluid Mech. 4, 149–190

Kinoshita, R. 1967: An analysis of the movement of flood waters by aerial photography, concerning characteristics of turbulence and surface flow. Photographic Surveying 6, 1–17 (in Japanese)

Kim, J.; Moin, P. 1980: Large eddy simulation of turbulent channel flow – Illiac IV calculation. AGARD CP 271, 14

Kovasznay, L. S. G.; Arman, A. 1957: Optical autocorrelation measurement of two-dimensional random patterns. Rev. Sci. Instrum. 28, 793

Kreplin, H. P. 1976: Experimentelle Untersuchungen der Längsschwankungen und der wandparallelen Querschwankungen der Geschwindigkeit in einer turbulenten Kanalströmung. PhD. Thesis, Georg-August-Universität zu Göttingen, F. R. Germany

Moin, P.; Kim, J. 1982: Numerical investigation of turbulent channel flow. J. Fluid Mech. 118, 341–377

Nezu, I. 1977: Turbulent structure in open-channel flows. Ph.D. Thesis, Kyoto University, Japan

Utami, T.; Blackwelder, R. F.; Ueno, T. 1990: Flow visualization and image processing of three-dimensional features of coherent structures in an open-channel flow. In: Near-wall turbulence. (ed. Kline, S. J.). pp. 289–305. New York: Hemisphere

Yano, M. 1983: Velocity measurement using correlation concerning with digital tracer image, flow visualization. Flow Visualzation Soc. of Japan 3, 189–192 (in Japanese)

Received April 3, 1990